# Study of effects of varying parameters on the dislocation density in 200 mm SiC bulk growth

**Sheng' ou Lu [1,3], Binjie Xu [2,3], Hongyu Chen [1], Wei Hang [1], Rong Wang [2,3], Julong Yuan [1,*], Xiaodong Pi [2,3,*] , Deren Yang [2,3], Xuefeng Han [2,3,*]**

[1] *Ultra-precision Machining Research Center, Zhejiang University of Technology, Hangzhou, Hangzhou 310023, China;*

[2] *State Key Laboratory of Silicon Materials & School of Materials Science and Engineering, Zhejiang University, Hangzhou 311200, China;*

[3] *Institute of Advanced Semiconductors & Zhejiang Provincial Key Laboratory of Power Semiconductor Materials and Devices, Hangzhou Global Scientific and Technological Innovation Center, Zhejiang University, Hangzhou, Zhejiang 310027, China*

\* Correspondence: xuefenghan@zju.edu.cn (X.H.); xdpi@zju.edu.cn (X.P.); jlyuan@zjut.edu.cn (J.Y.)

**Abstract:** Physical vapor transport is the dominant method for growing 200 mm SiC crystals, and the crystals produced by this method still have dislocations, which affect the performance of the device. In this study, the finite element analysis of 200 mm SiC crystal growth has been conducted to investigate the influencing parameters on the dislocations. The calculations are based on the model of multiple resistance heating proposed in our previous work. The transient heat transfer process for crystal growth has been calculated. Then dynamic mesh technique was employed to consider the shape evolution of the ingot during the crystal growth process. Finally, the distributions of the internal stress and dislocation density have been obtained based on the Alexander-Haasen model. The comparison of different parameters provides guidance for reducing the thermal stress and dislocation density in the 200 mm SiC crystal growth.

**Keywords**: SiC; Computer simulation; Growth from vapor; Dislocation density; Alexander-Haasen model

# 1.Introduction

4H-silicon carbide (SiC), with its superior properties such as high breakdown field

strength, high thermal conductivity, and high carrier mobility, is a promising wide-bandgap (WBG) semiconductor material for high-temperature, high-frequency, and high-power electronic devices [1-5]. The physical vapor transport (PVT) method is currently the most mature method for growing bulk SiC crystals. Crystals grown by the PVT method usually have defects such as micropipes, dislocations, cracks, etc. The micropipe is the most destructive defect in SiC crystals, and its presence increases leakage current and decreases breakdown voltage, leading to device failure [6]. Up to now, the micropipe density (MPD) has been dramatically reduced in SiC crystals. According to the literature, the micropipe density has been reported to reduce by 90% in 200 mm substrates [7, 8]. The industry has achieved "zero micropipe density" 4H-SiC single crystal substrate preparation. Overall, the micropipe is no longer an obstacle limiting the performance of SiC materials. Instead, dislocations should be more of our concern during crystal growth. Generally, dislocation density is regarded as an essential index to evaluate the quality of a SiC single crystal.

Currently, industrial production of SiC crystal size is mainly concentrated in 150 mm (6 inches). The crystal size of the further expansion can reduce the device cost. An increase of 50 mm in the wafer diameter corresponds to a 78% larger area and a potential increase in the number of devices per wafer of the same amount [9]. However, with the diameter increase from 150 mm to 200 mm, the difficulty of multiple physical field control increases, especially the thermal field control, which plays a decisive role in the growth of large-size SiC crystals [10]. As crystal growth by PVT is carried out under a thermal gradient, remarkable thermal stress is induced in a crystal by nonlinear thermal gradients during the growth process. As the crystal size increases, the thermal gradient increases. Consequently, the stresses should be studied carefully during 200 mm crystal growth since thermal stresses cause most dislocations.

To better understand the role of dislocations in the crystal growth process, Jordan et al. [11] proposed a parameter for the qualitative estimation of dislocation density $\sigma_{ex}$ for the first time. Compared to qualitative estimation, quantitative assessment of dislocation density provides more helpful information on single crystal quality. In quantitative analysis, the Alexander-Haasen (AH) model is used as the constitutive equation to calculate the relation between the time-dependent plastic strain and the dislocation density. The model was first used to calculate the dislocation density in the silicon ribbon [12]. Afterward, the model was also used to analyze dislocation density in III–V compound semiconductor crystals, such as GaAs and InP [13]. B. Gao et al.[14] have demonstrated through simulations and experiments that the AH model is also applicable to the plastic deformation of IV-IV compound semiconductor materials such as SiC. There is already literature on using the AH model to calculate the dislocation density of SiC crystals [15-18]. However, there has been little reported research on calculating thermal stresses and dislocations in 200 mm SiC. In our previous study [10], multiple resistance heating for SiC crystal growth has been proposed, and numerical calculations have been carried out. Machine learning has been utilized to optimize thermal field structure parameters favorable for high-quality crystal growth.

In this study, the finite element analysis of 200 mm SiC crystal growth has been carried out by using COMSOL Multiphysics based on our previous model, and the

dynamic mesh technique has been adopted to capture the shape evolution of ingot during the crystal growth process and simulate the distribution of the internal stress and dislocation density of the crystals under different growth conditions to provide guidance to the growth of 200 mm SiC crystal with high quality.

# 2.Numerical Model and Methods

## 2.1 Geometric model

**Fig. 1(a)** is a 2D axis-symmetric global model for the designed multiple resistance heating furnace of a SiC single crystal [10]. The model includes the following components: SiC powder, graphite crucible, SiC seed, seed holder, graphite foam insulation, and three resistance heaters, which are separated by graphite foam insulations. The furnace is filled with argon gas at a fixed pressure of 100 Pa. Compared to conventional induction coil heating, the advantage of multiple resistance heating is that the thermal radiation in the SiC powder region, the SiC seed region, and the seed holder region can be directly changed by varying the power distribution of the three heaters, thus allowing for more flexible control of the thermal field distribution. **Fig. 1(b)** shows the schematic diagram of each parameter that can be adjusted in this model; among them, $P_1$, $P_2$, and $P_3$ denote the power of the three heaters, Y represents the distance between the seed and the powder, and the value of Y also explains the amount of SiC powder. H denotes the height of the graphite crucible, which is also used to change the thermal field by adjusting the position of the crucible.



| (a) | (b) |
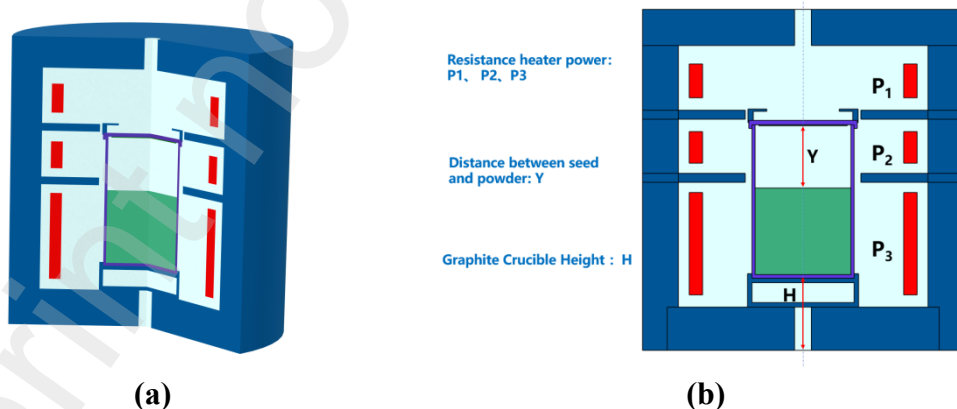
**Fig. 1** Crystal growth system in finite element calculations: **(a)** configuration of the multiple resistance heating furnace [10]; **(b)** schematic diagram of each parameter that can be adjusted in this model

The transient thermal field of crystal growth was firstly calculated; simultaneously, the shape of the crystal growth surface was updated in real-time according to the growth rate in conjunction with the dynamic mesh technique. After obtaining the crystal shape, the stress distribution in SiC ingots was calculated by reconfiguring and encrypting the crystal mesh. Finally, the dislocation density in the crystal was determined using the

Alexander-Haasen model until the convergence of results. **Fig.2** depicts the sequential calculation procedure. In the subsequent subsections, the principles governing the modeling of thermal, stress, and dislocation fields along with their corresponding equations and boundary conditions will be introduced.
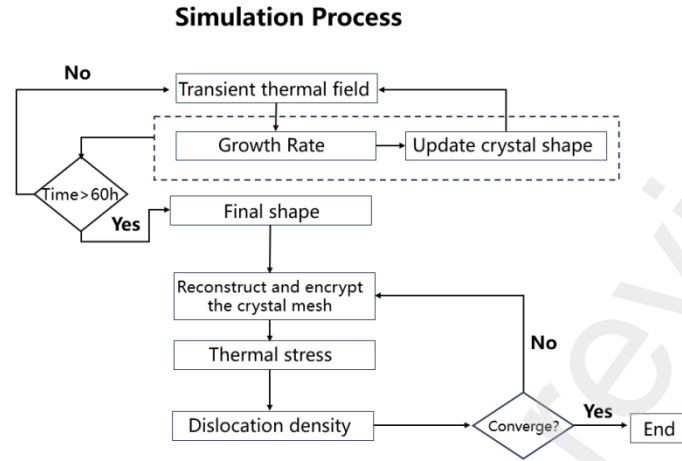


**Fig. 2** The operation flow chart of the simulation

## 2.2 Heat transfer

When employing the PVT method for SiC crystal growth, heat is transferred to the SiC powder via conduction and radiation, leading to its decomposition into gaseous components. Within the growth chamber, the diffusion facilitates the transportation of these gas phase constituents alongside latent heat associated with phase transition at the interface between SiC powder sublimation and deposition onto the seed crystal.

Despite the intricate chemical reactions taking place at the surfaces of both the powder and seed, it is feasible to approximate the alterations in these two characteristics as phase transitions of the SiC components. This equation (1) enables us to precisely calculate the latent heat at the interface

$$q_L = \rho v L \tag{1}$$

where $q_L$ is the released heat per unit area during the crystallization; $\rho$ is the density of SiC; $v$ is the crystal growth rate and $L$ is the latent heat of deposition with a value of 5730 $kJ/kg$ [10].

Since the temperature is above 2000 K, the effect of radiative heat transfer is significant and needs to be considered. The radiative heat flux at the wall is calculated under the heat transfer wall boundary condition as follows:

$$q_w = \varepsilon\sigma\left(T_{amb}^4 - T_w^4\right) \tag{2}$$

where $\sigma$ is the Stefan-Boltzmann constant; $T_{amb}$ is the ambient temperature; $T_w$ is wall temperature and $\varepsilon$ is the wall emissivity.

Without accounting for convective heat transfer, the impact of latent heat is deemed insignificant in comparison to radiant heat. The transient heat transfer equation, which only considers conduction and radiation while neglecting convective heat

transfer in the thermal field calculation of the system, can be expressed as follows:

$$\rho C_p \frac{\partial T}{\partial t} + \nabla \cdot (-k\nabla T) = Q \tag{3}$$

The material properties in the thermal field calculation can be found in Table 1

**Table.1** Material properties related to heat transfer calculation [19]

| Properties | Value and unit |
|---|---|
| Density of the graphite crucible | $1730 \text{ kg/m}^3$ |
| Density of the insulation layer | $200 \text{ kg/m}^3$ |
| Density of 4H-SiC crystal | $3220 \text{ kg/m}^3$ |
| Heat capacity of the graphite crucible | $2250 \text{ J/(kg} \cdot \text{K)}$ |
| Heat capacity of the insulation layer | $1000 \text{ J/(kg} \cdot \text{K)}$ |
| Heat capacity of the 4H-SiC crystal | $1281 \text{ J/(kg} \cdot \text{K)}$ |
| Thermal conductivity of the graphite crucible | $22.3 + (2.3 \times 10^7)/(1 + (T/0.00056)) \text{ W/(m} \cdot \text{K)}$ |
| Thermal conductivity of the insulation layer | $0.193 \times exp(0.00079 \times (T - 273)) \text{ W/(m} \cdot \text{K)}$ |
| Thermal conductivity of 4H-SiC crystal | $4.517 \times 10^5/(T^{1.29}) \text{ W/(m} \cdot \text{K)}$ |
| Emissivity of the wall | 0.8 |
| Emissivity of the graphite crucible | 0.8 |
| Emissivity of the insulation layer | 0.8 |
| Emissivity of the 4H-SiC crystal | 0.8 |

# 2.3 Crystal Growth Interface

During the process of SiC crystal growth, sublimation of SiC powders occurs at high temperatures, resulting in a gas phase consisting of Si, $Si_2C$, and $SiC_2$. Through a convection-diffusion mechanism driven by temperature and concentration gradients within the growth chamber, these vapor species are transported to the seed surface where they create a supersaturated condition near the ingot surface leading to their deposition on the seed [20]. The primary reactions taking place on the seed's surface involve:

$$SiC_2(g) + \text{Si}(g) \Leftrightarrow 2\text{SiC}(s) \tag{4}$$

$$\text{Si}_2\text{C}(g) \Leftrightarrow \text{SiC}(s) + \text{Si}(g) \tag{5}$$

where the labels $(s)$ and $(g)$ denote solids and gases, respectively.

It has been reported in the literature that $SiC_2$ and Si are the predominant gas species responsible for determining the crystal growth rate at temperatures below and above 2900 K, respectively [21]. Typically, SiC crystals are grown at temperatures below 2900 K, thus establishing $SiC_2$ as the dominant gas species influencing the growth rate. The molar flux of $SiC_2$ on the seed surface and its corresponding growth rate can be accurately described using the Hertz-Knudsen theoretical framework：

$$J_{SiC_2} = \alpha_i \frac{\left(P_{SiC_2} - P_{SiC_2}^*(T(r))\right)}{\sqrt{\left(2\pi M_{SiC_2}RT(r)\right)}} \tag{6}$$

$$v_g = 2(M_{SiC}/\rho_{SiC})J_{SiC_2} \tag{7}$$

where $\alpha_i$ is the adsorption coefficient; $P_{SiC_2}$ is partial pressure of SiC$_2$ (unknown value); $T(r)$ is radial temperature of seed surface; $P_{SiC_2}^*$ is equilibrium vapor pressures of SiC$_2$ provided by Lilov (1993) [21]; $M$ and $R$ are the molar mass of the gas species and the ideal gas constant, respectively.

To determine the value of $P_{SiC_2}$ in Eq. (6), the problem can be approached in a simplified way. **Fig. 3** shows a physical model of PVT growth of SiC crystals. The coordinate system offers the pressure P along the axial coordinate z. It is assumed that at the powder surface, the pressure of the gas-phase component SiC$_2$ is approximated to be equal to the thermodynamic equilibrium pressure corresponding to the average temperature at the powder surface（A-B）, and the partial pressure of SiC$_2$ inside the growth chamber is considered to be equal to $P_{SiC_2}^*(T_{powder})$.
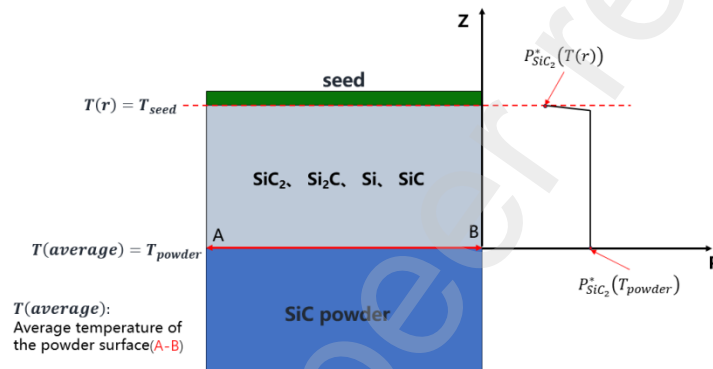


**Fig. 3** Physical model of PVT growth of SiC.

To determine the growth rate, the model assumes the following:

1. It neglects mass transfer effects and only considers temperature impact;

2. It exclusively focuses on axial crystal growth while neglecting radial growth;

3. It does not consider any influence of powder consumption on heat field distribution.

We aim to incorporate a dynamic mesh physical field into our model to accurately simulate the shape variations that occur during crystal growth. To illustrate this setup, a simplified schematic is presented in **Fig. 4(a)**, where the SiC seed portion of the grid is divided into 50×5 grid cells, while the remaining area consists of a free triangle grid. In **Fig. 4(b)**, a schematic representation of a graphite crucible within a simplified 2D axisymmetric PVT growth system is depicted. The grids on the upper surface of both the seed and powder are fixed ($u_r = u_z = 0$), whereas those on the symmetry axis and sidewalls of the crucible allow for slip ($u_r = 0$). Furthermore, on the bottom surface of the seed, grids are set with a velocity in z-direction equal to $v_g$. **Fig. 4(c)** visually demonstrates both grid movement and changes in crystal dislocation density over time from 0 to 60 hours during computation.
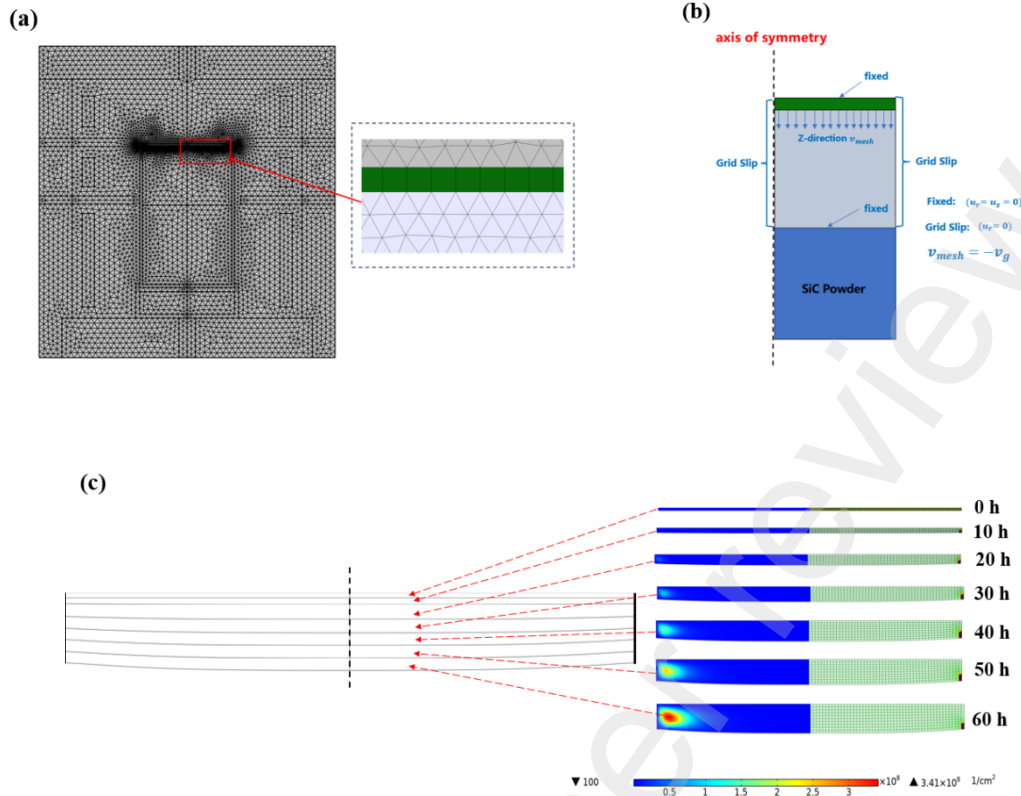
**Fig. 4** The schematic diagram for setup of the model dynamic mesh：**(a)** the meshing of the calculation model; **(b)** dynamic mesh boundary conditions; **(c)** changes in dislocation density during mesh movement

## 2.4 Thermal stress and dislocation density

The governing equations for calculating thermal stresses include force equilibrium, geometric equations, and the constitutive relation. Continuous temperature variation within a solid generally generates thermal stresses. According to the linear thermal stress theory, the components of the strain tensor are a linear function of the stress tensor, and temperature variation generates these components. Hooke's law and stress-strain relations for elastic and thermal strains are given by:

$$\sigma_{ij} = C_{ijkl}(\varepsilon_{kl} - \alpha\theta\delta_{kl}), (\theta = T - T_0) \tag{8}$$

where $\sigma_{ij}$ is the stress tensor; $C_{ijkl}$ is the elastic constant tensor which depends on crystal structure; $\alpha$ is thermal expansion coefficients; $\varepsilon_{kl}$ and $\delta_{kl}$ are the strain tensor and Kronecker delta tensor, respectively.

The 4H-SiC single crystal has a hexagonal structure, so its elastic matrix has only five independent components. Assuming $T_0 = 293.15K$, the stress-strain relation in the 2D axisymmetric can be represented as:

$$\begin{pmatrix} \sigma_{rr} \\ \sigma_{\theta\theta} \\ \sigma_{zz} \\ \sigma_{rz} \end{pmatrix} = \begin{pmatrix} C_{11} & C_{12} & C_{13} & 0 \\ C_{12} & C_{11} & C_{13} & 0 \\ C_{13} & C_{13} & C_{33} & 0 \\ 0 & 0 & 0 & C_{44} \end{pmatrix} \begin{pmatrix} \varepsilon_{rr} - \alpha(T - T_0) \\ \varepsilon_{\theta\theta} - \alpha(T - T_0) \\ \varepsilon_{zz} - \alpha(T - T_0) \\ \varepsilon_{rz} \end{pmatrix} \tag{9}$$

According to Zhang et al. [22], an isotropic temperature-dependent thermal expansion coefficient $\alpha(T)$ is considered:

$$\alpha(T) = -5.54 \cdot 10^{-6} \text{K}^{-1} \exp\left(-\frac{T}{3358.8\text{K}}\right)$$
$$- 2.78 \cdot 10^{-4} \text{K}^{-1} \exp\left(-\frac{T}{42.3\text{K}}\right) + -8.83 \cdot 10^{-6} \text{K}^{-1} \tag{10}$$

The temperature field of SiC crystals grown by PVT can be approximated as a 2D axisymmetric distribution. Therefore, the displacement distribution resulting from the thermal expansion of the crystals can also be considered as a 2D axisymmetric distribution. Consequently, the relationship between strain and displacement can be expressed as follows:

$$\boldsymbol{\varepsilon} = \frac{1}{2}[\nabla \boldsymbol{u} + (\nabla \boldsymbol{u}^T)] \tag{11}$$

And in the cylindrical coordinate system $\nabla = \frac{\partial}{\partial r}\boldsymbol{e}_r + \frac{1}{r}\frac{\partial}{\partial\theta}\boldsymbol{e}_\theta + \frac{\partial}{\partial z}\boldsymbol{e}_z$, strain components [23] can be obtained as Eq. (9):

$$\varepsilon_{rr} = \frac{\partial u_r}{\partial r}, \varepsilon_{\theta\theta} = \frac{u_r}{r}, \varepsilon_{zz} = \frac{\partial u_z}{\partial z},$$
$$\varepsilon_{rz} = \frac{1}{2}\left(\frac{\partial u_r}{\partial z} + \frac{\partial u_z}{\partial r}\right), \varepsilon_{r\theta} = \varepsilon_{\theta z} = 0 \tag{12}$$

where $u_r$ and $u_z$ are the displacement in the radial direction and the displacement in the axial direction, respectively. Based on the assumption of 2D axisymmetric, the displacement in the angular direction is zero.

The equation of force equilibrium at steady state without external force are described as:

$$\nabla \cdot \boldsymbol{\sigma} = 0 \tag{13}$$

and in the cylindrical coordinate system with 2D axisymmetric condition can be followed as [24]:

$$\frac{\partial \sigma_{rr}}{\partial r} + \frac{\partial \sigma_{rz}}{\partial z} + \frac{\sigma_{rr} - \sigma_{\theta\theta}}{r} = 0$$
$$\frac{\partial \sigma_{rz}}{\partial r} + \frac{\partial \sigma_{zz}}{\partial z} + \frac{\sigma_{rz}}{r} = 0 \tag{14}$$

The Von Mises stress is used to represent the stress components:

$$\sigma_{von} = \left(\frac{3}{2}S_{ij}S_{ij}\right)^{1/2} \tag{15}$$

where $S_{ij}$ is the stress deviator, $S_{ij} = \sigma_{ij} - \frac{1}{3}\sigma_{kk}\delta_{ij}$.

For the calculation of the thermal stress field in SiC crystals, the boundary conditions are described as follows：

(a) Considering the seed attached to the seed holder, the displacement boundary

conditions on the upper surface of the seed are set to be $u_z = 0$;

(b) Neglecting the effect of growing polycrystals on the growth surface, the stress boundary conditions on growth surface can be described as $\boldsymbol{\sigma} \cdot \boldsymbol{n} = 0$.

The material properties in the thermal stress calculation can be found in Table 2

**Table.2** Material properties related to thermal stress calculation [25]

| Symbol | Description | Value and Unit |
|---|---|---|
| $C_{11}$ | Elasticity constants | $-0.025\ GPa \times T + 486.6\ GPa$ |
| $C_{12}$ | Elasticity constants | $-0.011\ GPa \times T + 101.3\ GPa$ |
| $C_{13}$ | Elasticity constants | $-0.011\ GPa \times T + 59.02\ GPa$ |
| $C_{33}$ | Elasticity constants | $-0.025\ GPa \times T + 528.9\ GPa$ |
| $C_{44}$ | Elasticity constants | $-0.007\ GPa \times T + 150.3\ GPa$ |

The dislocation generation or nucleation determines the first existing dislocations. However, the dislocation multiplication, driven by the thermal stress, determines the final dislocations in the as-grown crystal. Therefore, thermal stress is the most critical factor in determining the presence of final dislocations [26].

For the elastoplastic crystal, the total strain consists of three components of strain:

$$\varepsilon_{ij} = \varepsilon_{ij}^e + \varepsilon_{ij}^T + \varepsilon_{ij}^{pl} \tag{16}$$

where $\varepsilon_{ij}^e$, $\varepsilon_{ij}^T$ and $\varepsilon_{ij}^{pl}$ are elastic strain, thermal strain, and plastic strain, respectively. The thermal strain has been considered in Eq. (8) and (9).

The main slip direction of the hexagonal SiC crystal is the $[11\bar{2}0]$ direction located in the (0001) plane. For the 2D axisymmetric case with the symmetry axis oriented along the $[0001]$ direction (c axis), without considering the anisotropic stress component $\sigma_{rz}$ is considered to be the resolved shear stress, then the stress-strain relationship with plastic can be rewritten in Eq. (9) to get：

$$\begin{pmatrix} \sigma_{rr} \\ \sigma_{\theta\theta} \\ \sigma_{zz} \\ \sigma_{rz} \end{pmatrix} = \begin{pmatrix} C_{11} & C_{12} & C_{13} & 0 \\ C_{12} & C_{11} & C_{13} & 0 \\ C_{13} & C_{13} & C_{33} & 0 \\ 0 & 0 & 0 & C_{44} \end{pmatrix} \begin{pmatrix} \varepsilon_{rr} - \alpha(T - T_0) \\ \varepsilon_{\theta\theta} - \alpha(T - T_0) \\ \varepsilon_{zz} - \alpha(T - T_0) \\ \varepsilon_{rz} - \varepsilon_{rz}^{pl} \end{pmatrix} \tag{17}$$

The Alexander-Haasen model [14] describes the time evolution of the mobile dislocation density $N_m$ and plastic strain $\varepsilon_{pl}^{(\alpha)}$ and the rate of the plastic strain is given by Orowan's equation:

$$\frac{d\varepsilon_{pl}^{(\alpha)}}{dt} = N_m^{(\alpha)} v^{(\alpha)} b \tag{18}$$

$$\frac{dN_m}{dt} = KvN_m\tau_{eff}^\lambda \tag{19}$$

$$v = k_0 \tau_{eff}^m exp\left(-\frac{Q}{k_bT}\right) \tag{20}$$

where $(\alpha)$ is the slip direction; $v$ is the slip velocity of dislocation; $\tau_{eff}$ is the effective stress representing the contribution of stress from dislocation; $b$ is Burger's vector; $Q$ is activation enthalpy; $k_b$ is Boltzmann constant; and $K, \lambda, m, k_0$ are constants related to materials. The expression for the effective stress can be expressed as a function of the

maximum value:

$$\tau_{eff} = max\left(\tau_a - D\sqrt{N_m} - \tau_{crit}, 0\right) \quad (21)$$

here $\tau_a$ is the resolved shear stress in the slip direction, in the case of 2D axisymmetric consideration, the resolved shear stress $\tau_a$ is found for the hexagonal crystals as the absolute magnitude of $\sigma_{rz}$; $D\sqrt{N_m}$ is the back-stress on a given dislocation due to the neighboring ones, which resists its movement through interaction; $\tau_{crit}$ is the back-stress caused by the interaction between dislocations and impurity atoms [27]; it should also be noted that dislocation density calculations require an initial dislocation density that is not zero because it can be seen from Eq. (15) that the rate of dislocation density is a self-multiplying equation. Here we set the initial dislocation density to $100\ cm^{-2}$, initial values within a certain range do not affect the value of the final dislocation density [28].

The material properties in the dislocation density calculation can be found in Table 3.

**Table.3** Material properties related to dislocation density calculation [7]

| Symbol | Description | Value and Unit |
|:------:|:-----------:|:--------------:|
| $b$ | Burger's vector | $3.073 \times 10^{-10}\ m$ |
| $\lambda$ | stress exponential factor | 1.1 at $T > 1000$ ℃<br>0.6 at $T < 1000$ ℃ |
| $m$ | stress exponential factor | 2.8 |
| $Q$ | activation enthalpy | 3.3 eV at $T > 1000$ ℃<br>2.6 eV at $T < 1000$ ℃ |
| $v$ | dislocation velocity | $m/s$ |
| $K$ | multiplication constant | $7.0 \times 10^5$ |
| $N_m$ | mobile dislocation density | $m^{-2}$ |
| $\tau_{eff}$ | effective stress | Pa |
| $\tau_{crit}$ | doping stress | Pa |
| $D$ | hardening factor [29] | $\dfrac{b(C_{11} - C_{13})}{4\pi(1 - v)}$ |
| $T$ | temperature | K |
| $k_0$ | material constant | $8.5 \times 10^{-15}$ |
| $k_b$ | Boltzmann constant | $8.615 \times 10^{-5}\ eV/K$ |

# 3. Results and discussion

## 3.1 The varying of power

The power distribution is crucial for the thermal field of the furnace. Our previous study explored the effect of different power distributions on RTD and ETG, as described in the literature [10]. In this study, by setting $P_{total} = P_1 + P_2 + P_3 = 27$ kW to ensure that the temperature on the seed surface is suitable for SiC crystal growth with parameters Y = 138 mm (distance between seed and powder) and H = 160 mm (crucible height). Using a constant power setting for one heater, while independently adjusting the power of the other two heaters, to investigate their impact on dislocation density during crystal growth. The detailed explanation of simulation results follows, elucidating our findings.

Firstly, the power distribution of heaters $P_1$ and $P_2$ is changed by fixing the power of heater $P_3$=19 kW. **Fig. 5 (a)–(c)** shows the $P_1$ and $P_2$ dependence on the temperature of the crystal after growing 60h for $P_1$+$P_2$=8 kW. The maximum temperature of the crystal increases as $P_2$ increases, while the minimum temperature exhibits an opposite trend. This is because heater $P_2$ directly heats the crucible wall on the side of the crystal through thermal radiation, significantly impacting its temperature. Additionally, there are variations in calculated crystal shapes and thicknesses for each of the three power cases. The thickness of the crystals increases with an increase in $P_2$. Among different
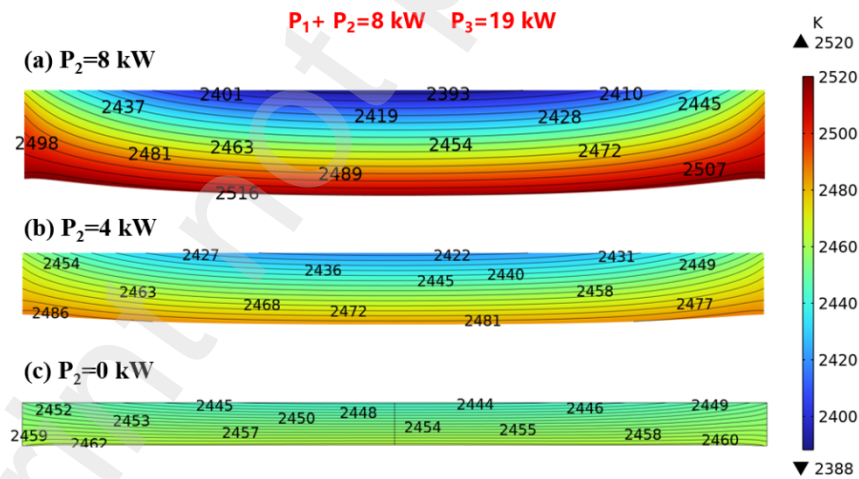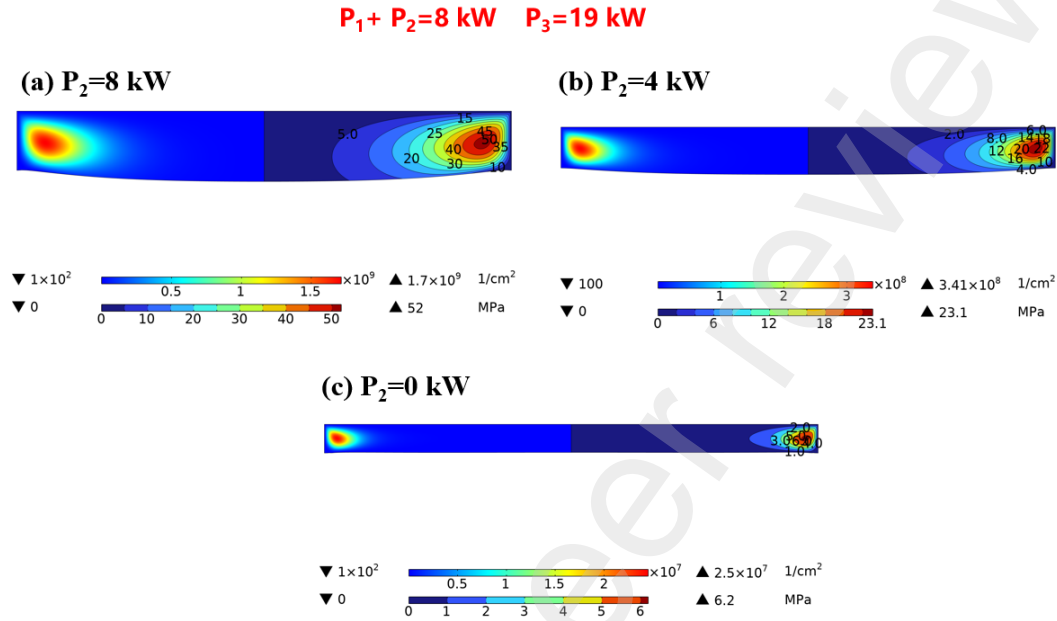


**Fig. 5** $P_1$ and $P_2$ dependence of temperature of crystal after growing 60h for $P_1 + P_2$=8 kW: **(a)** $P_2$=8 kW; **(b)** $P_2$=4 kW;**(c)** $P_2$=0 kW

values of $P_2$, 8 kW results in crystals with the most convex shape, 0 kW leads to concave crystals, and 4 kW lies in between. The shape of the crystals significantly affects the stresses, and typically, convex crystals generate more significant thermal stresses. **Fig. 6 (a)–(c)** shows the $P_1$ and $P_2$ dependence of dislocation density(left) and the absolute value of shear stress $|\sigma_{rz}|$(right) of crystal after growing 60h for $P_1$+$P_2$=8 kW. The maximum value of the dislocation density increases as $P_2$ increases. The difference in

dislocation density between convex and concave crystals is two orders of magnitude. The minimum dislocation density is 100 $(cm^{-2})$, because the initial value is 100 $(cm^{-2})$ and if $|\sigma_{rz}| - D\sqrt{N_m} < 0$ then dislocation proliferation rate $dN_m/dt = 0$. It can also be expected that the trend of stress distribution will align with that of the dislocation density, as shear stress serves as a driving force for dislocation proliferation in the AH model.

$P_1 + P_2 = 8$ kW    $P_3 = 19$ kW

(a) $P_2 = 8$ kW

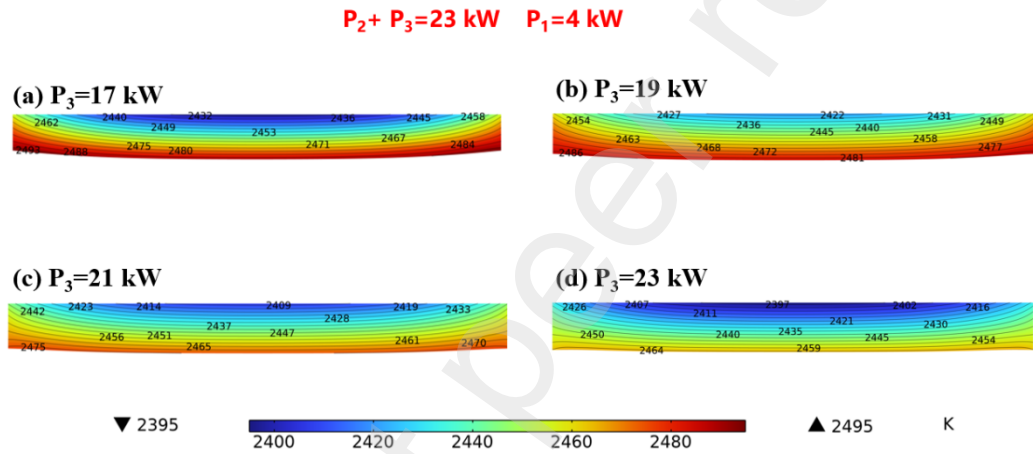(b) $P_2 = 4$ kW

(c) $P_2 = 0$ kW



**Fig. 6** $P_1$ and $P_2$ dependence of dislocation density(left) and the absolute value of shear stress $\sigma_{rz}$

(right) of crystal after growing 60h for $P_1 + P_2 = 8$ kW: **(a)** $P_2 = 8$ kW; **(b)** $P_2 = 4$ kW;**(c)** $P_2 = 0$ kW

Secondly, the power distribution of heaters $P_1$ and $P_3$ is adjusted by fixing the power of heater P2 at 4 kW and ensuring that the combined power of $P_2$ and $P_3$ exceeds 20 kW in order to maintain a higher temperature for the SiC powder compared to the seed. **Fig. 7 (a)–(d)** illustrates the dependence of $P_1$ and $P_3$ on the crystal's temperature after growing for 60 hours with a total power input of $P_1+P_3 = 23$ kW. The effect of $P_3$ on the crystal temperature in this case exhibits the same trend as that of $P_2$ in the first case, and all calculated crystal shapes are convex. Additionally, as $P_3$ increases, the thickness of crystals becomes larger. This is because heater $P_3$ can heat the crucible wall
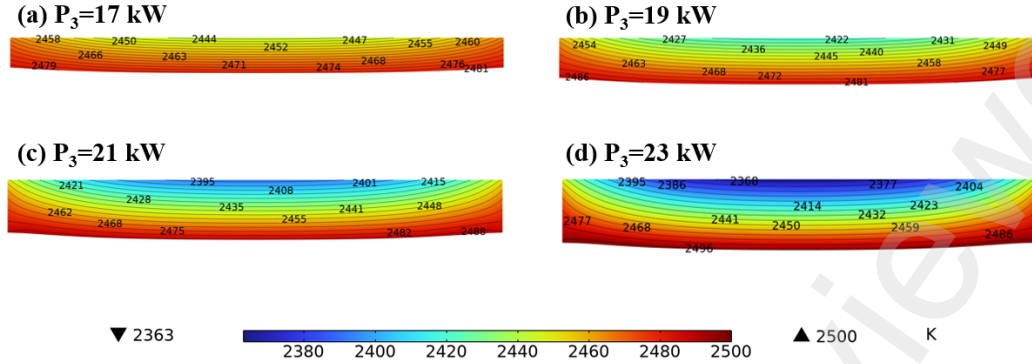
**Fig. 7** $P_1$ and $P_3$ dependence of temperature of crystal after growing 60h for $P_1 + P_3$=23 kW: **(a)** $P_3$=17 kW; **(b)** $P_3$=19 kW;**(c)** $P_3$=21 kW;**(d)** $P_3$=23 kW
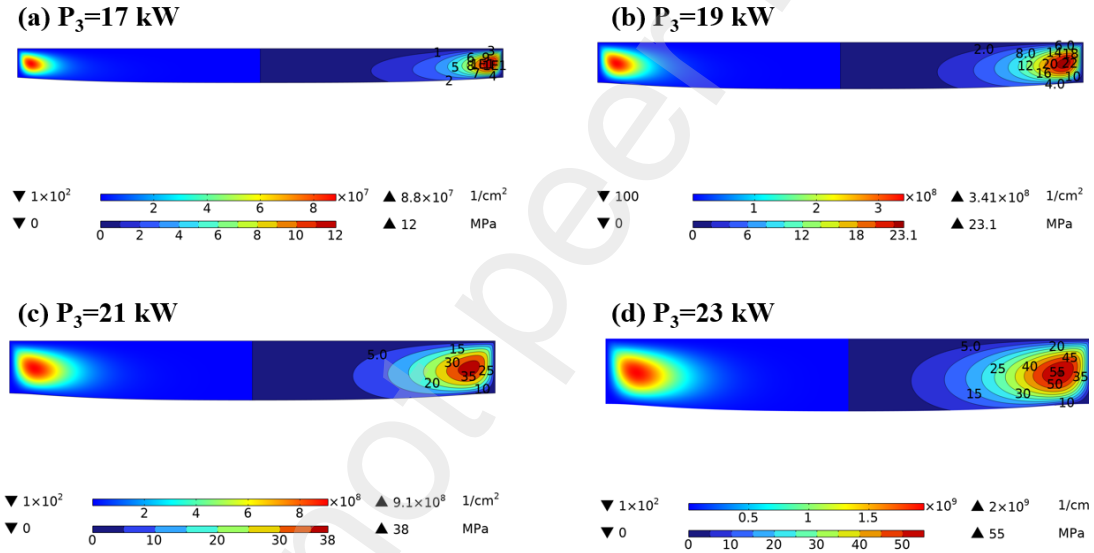


**Fig. 8** $P_1$ and $P_3$ dependence of dislocation density(left) and the absolute value of shear stress $\sigma_{rz}$ (right) of crystal after growing 60h for $P_1 + P_3$=23 kW: **(a)** $P_3$=17 kW; **(b)** $P_3$=19 kW;**(c)** $P_3$=21 kW;**(d)** $P_3$=23 kW

on the side wall of SiC powder through thermal radiation. As a result, with an increase in $P_3$, there is a greater temperature difference between the powder and seed which leads to an increased growth rate of crystals. **Fig. 8 (a)–(d)** shows the $P_1$ and $P_3$ dependence of dislocation density(left) and the absolute value of shear stress $|\sigma_{rz}|$(right) of crystal after growing 60h for $P_1+P_3$=23 kW. The maximum value of the dislocation density increases as P3 increases. Despite all crystals being convex, the temperature gradient also increases with increasing crystal thickness, resulting in a nearly fivefold difference in the maximum shear stress and two orders of magnitude difference in the maximum dislocation density.

Finally, the power distribution of heaters $P_2$ and $P_3$ is adjusted by setting the power of heater $P_1$ to 4 kW and ensuring that the power of heater $P_3$ is greater than 16 kW, in

order to maintain a higher temperature for the SiC powder compared to the seed. **Fig. 9 (a)–(d)** illustrates the relationship between $P_2$ and $P_3$ with respect to the crystal's temperature after a growth period of 60 hours, where $P_2+P_3$=23 kW. As $P_3$ increases, the temperature of the crystal decreases; however, there is an increasing disparity between the maximum and minimum temperatures. **Fig. 10 (a)–(d)** shows the $P_2$ and $P_3$ dependence of dislocation density(left) and the absolute value of shear stress (right) of crystal after growing 60h for $P_2+P_3$=23 kW. The maximum values of shear stress and dislocation density for the four cases do not differ much, and the dislocation density orders of magnitude are all in the order of 8 of 10. From the previous analysis, it can be seen that both $P_2$ and $P_3$ are positively correlated with the value of maximum shear stress in the crystal. It can be deduced from **Fig. 10** that the influence of $P_3$ is more significant than that of $P_2$ because the result at $P_3$=23 kW and $P_2$=0 kW is more significant than that at $P_3$=17kw and $P_2$=6kw. However, the influence of $P_2$ on the convexity of the crystal is the greatest.

**$P_2+ P_3$=23 kW    $P_1$=4 kW**



**Fig. 9** $P_2$ and $P_3$ dependence of temperature of crystal after growing 60h for $P_2 + P_3$=23 kW: **(a)** $P_3$=17 kW; **(b)** $P_3$=19 kW;**(c)** $P_3$=21 kW;**(d)** $P_3$=23 kW
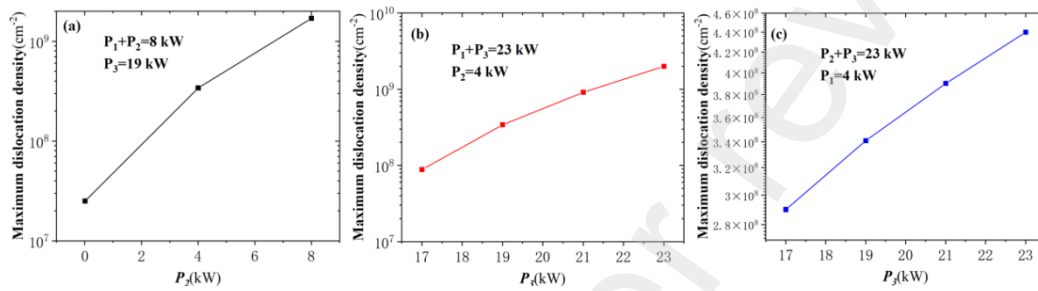
**$P_2+ P_3$=23 kW    $P_1$=4 kW**
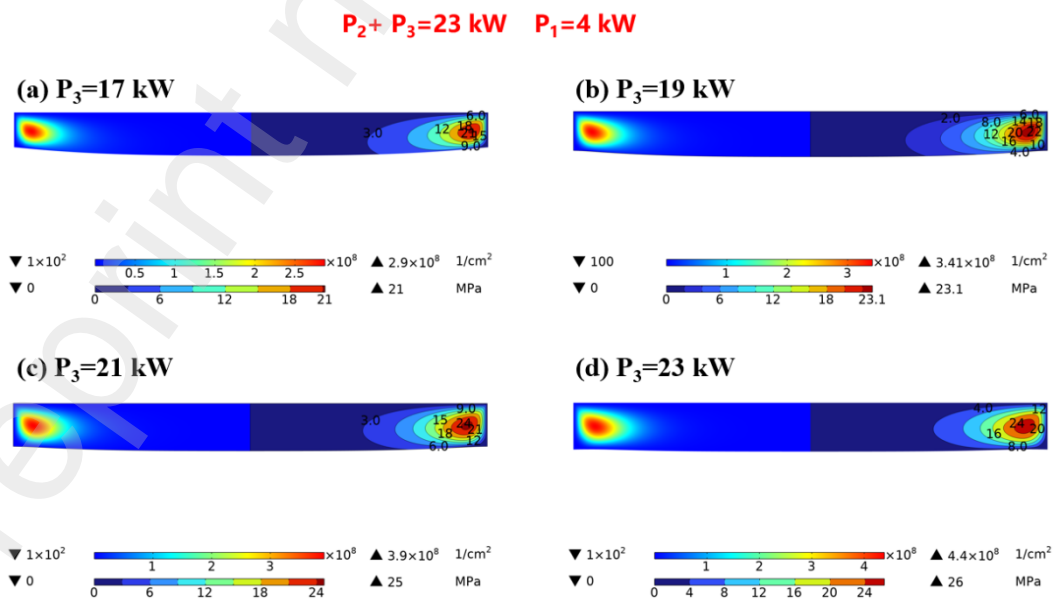


**Fig. 10** $P_2$ and $P_3$ dependence of dislocation density(left) and the absolute value of shear stress

$\sigma_{rz}$(right) of crystal after growing 60h for $P_2 + P_3$=23 kW: **(a)** $P_3$=17 kW; **(b)** $P_3$=19 kW;**(c)** $P_3$=21 kW;**(d)** $P_3$=23 kW

**Fig. 11 (a)-(c)** shows the correlation between heater power distribution and the maximum dislocation density of the grown crystal. By simulating the power, we can draw the following conclusions:

1. The maximum stress and thickness of the growing crystal are negatively correlated with $P_1$ and positively correlated with $P_2$ and $P_3$;

2. $P_3$ has a greater impact on the maximum stress than $P_2$;

3. $P_2$ has a stronger effect on crystal convexity than $P_3$.



**Fig. 11** The correlation of heater power distribution and the maximum dislocation density of the grown crystal:**(a)** $P_1 + P_2$=8 kW, $P_3$=19 kW;**(b)** $P_1 + P_3$=23 kW, $P_2$=4 kW;**(c)** $P_2 + P_3$=23 kW, $P_1$=4 kW

## 3.2 The varying of crucible height

In the multiple resistance heating model, the magnitude of thermal radiation in the SiC powder, seed crystal, and seed crystal holder regions can be varied by adjusting different crucible heights. To investigate the effect of varying crucible height on the maximum value of stress in the grown crystal, the power of heaters is considered to be $P_1$=$P_2$=4kW and $P_3$=19kW the power for heaters, while treating crucible height (H) as a variable for calculation. **Fig. 12 (a)–(f)** illustrates how crucible height (H) affects the temperature of the crystal after growing for 60 hours. As the crucible position increases, the temperature of the growing crystals decreases. The reason for this can be explained as follows: The heat in the SiC powder mainly originates from the thermal radiation of Heater 3. However, as the crucible position increases, there is a weakening in the thermal radiation between Heater 3 and the side wall of the crucible where the powder is located.
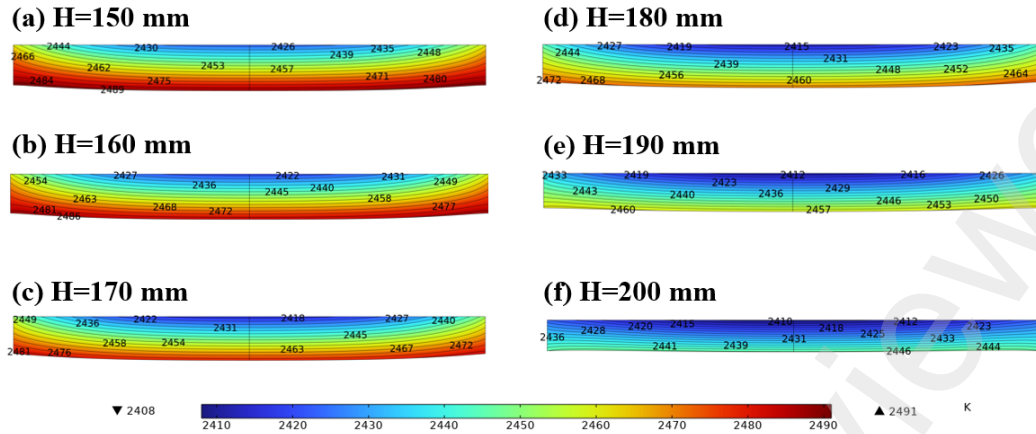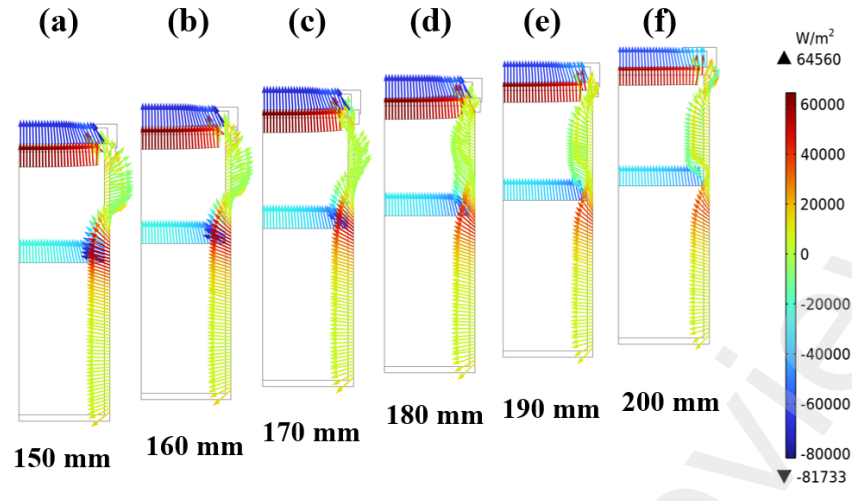
**Fig. 12** The crucible height (H) dependence of the temperature of the crystal after growing 60h:

**(a)** 150mm; **(b)** 160mm; **(c)** 170mm; **(d)** 180mm; **(e)** 190mm; **(f)** 200mm;

**Fig.13 (a)–(f)** shows the heat flux in the growth chamber, with the arrow indicating the direction of heat transfer and the color representing surface radiance. Positive values indicate radiative heat transfer into the solid, while negative values indicate heat transfer into the gas domain. As shown in the figure, an increase in crucible height results in a gradual decrease in radiant heat flux on the side wall of the crucible containing SiC powder. However, there is no significant difference in the color of the arrows when H ranges from 150 to 170 mm. At this point, the heat flux of the crucible sidewall of the growth crystal undergoes changes and a portion of the heat starts to be transferred inward. As the position of the crucible continues to increase, there is a noticeable alteration in radiation below, while all the heat within the crucible sidewall is transferred inward. **Fig. 14** illustrates the distribution of radial temperature gradient in crystals at various crucible heights. It is evident that the pattern of the radial temperature gradient remains consistent, however, its numerical value decreases as the height of the crucible increases. The non-uniform distribution of the radial temperature gradient is the primary cause for the increase in shear stress, and the formation of shear stress is primarily influenced by radial temperature gradients [30].

**Fig. 15 (a)–(f)** show the dislocation density(left) and the absolute value of shear stress $\sigma_{rz}$(right) of the crystal after growing 60 h at various crucible heights (H). Crucible height variations do not affect the maximum thermal stress to the same significant extent as power variations. The orders of magnitude of the maximum dislocation densities are all in $10^8$. However, there is some difference in the shape and thickness of the grown crystals, with the convexity and thickness of the crystals grown in the low crucible position being more significant than in the high crucible position. **Fig. 16** shows the correlation of crucible height(H) and the maximum dislocation density of the grown crystal.
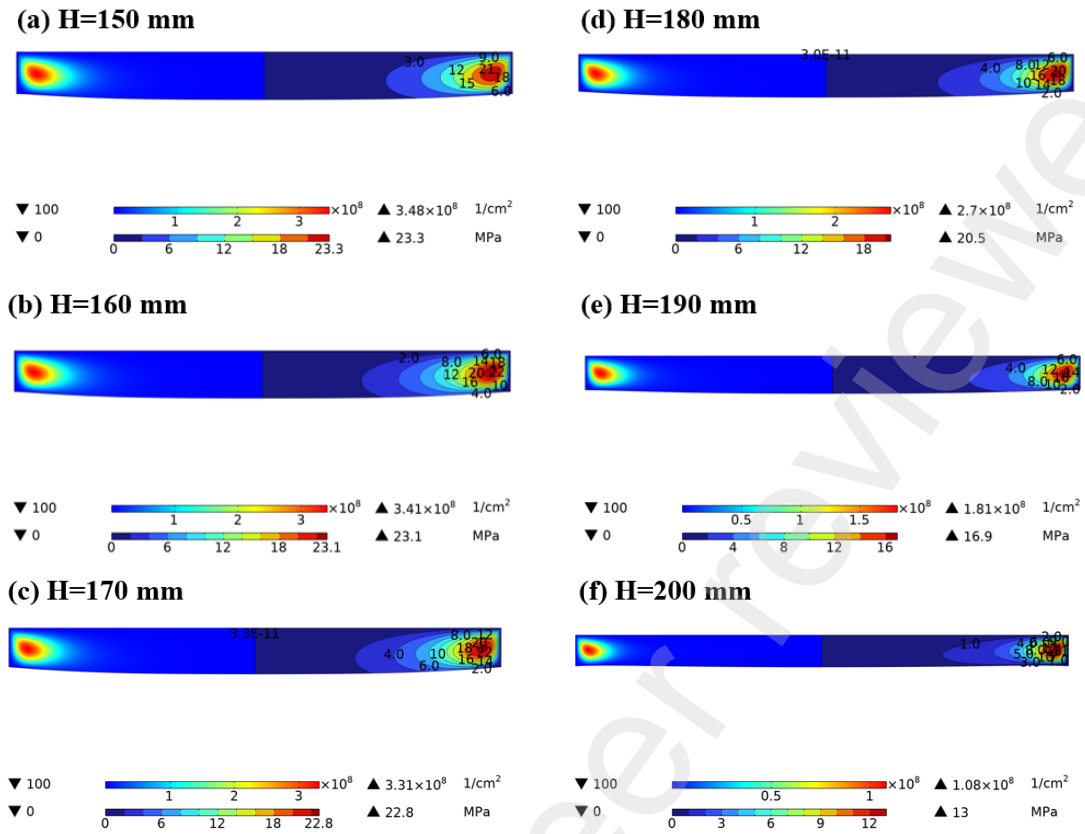
**Fig. 13** Heat flux in the growth chamber at various crucible height(H):**(a)** 150mm; **(b)** 160mm; **(c)** 170mm; **(d)** 180mm; **(e)** 190mm; **(f)** 200mm.
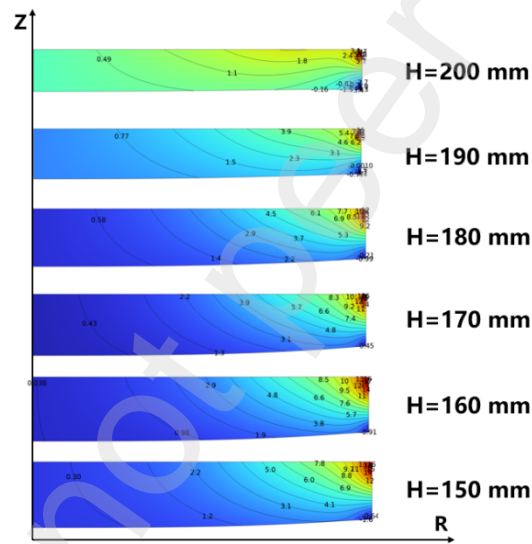


**Fig. 14** Radial temperature gradient of crystal after growing 60h at various crucible height(H)

**(a) H=150 mm**



▼ 100　▼ 0　　×10⁸　▲ 3.48×10⁸ 1/cm²　▲ 23.3 MPa

**(b) H=160 mm**



▼ 100　▼ 0　　×10⁸　▲ 3.41×10⁸ 1/cm²　▲ 23.1 MPa

**(c) H=170 mm**



▼ 100　▼ 0　　×10⁸　▲ 3.31×10⁸ 1/cm²　▲ 22.8 MPa

**(d) H=180 mm**



▼ 100　▼ 0　　×10⁸　▲ 2.7×10⁸ 1/cm²　▲ 20.5 MPa

**(e) H=190 mm**



▼ 100　▼ 0　　×10⁸　▲ 1.81×10⁸ 1/cm²　▲ 16.9 MPa

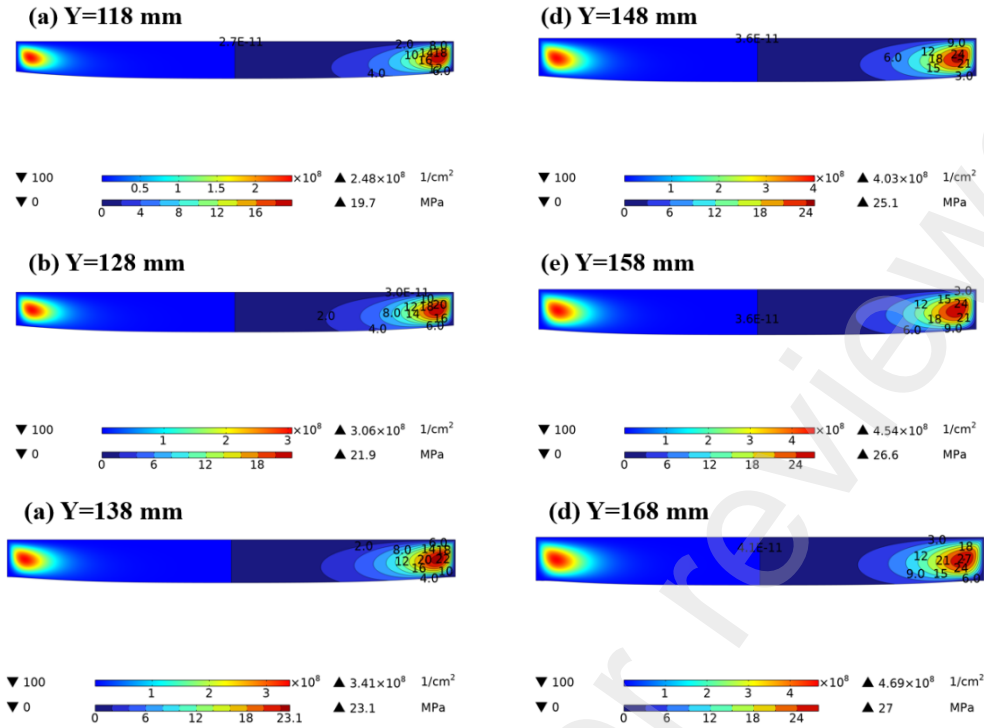**(f) H=200 mm**



▼ 100　▼ 0　　×10⁸　▲ 1.08×10⁸ 1/cm²　▲ 13 MPa

**Fig. 15** Dislocation density(left) and the absolute value of shear stress $\sigma_{rz}$(right) of crystal after growing 60h at various crucible height(H):**(a)** 150mm; **(b)** 160mm; **(c)** 170mm; **(d)** 180mm; **(e)** 190mm; **(f)** 200mm.
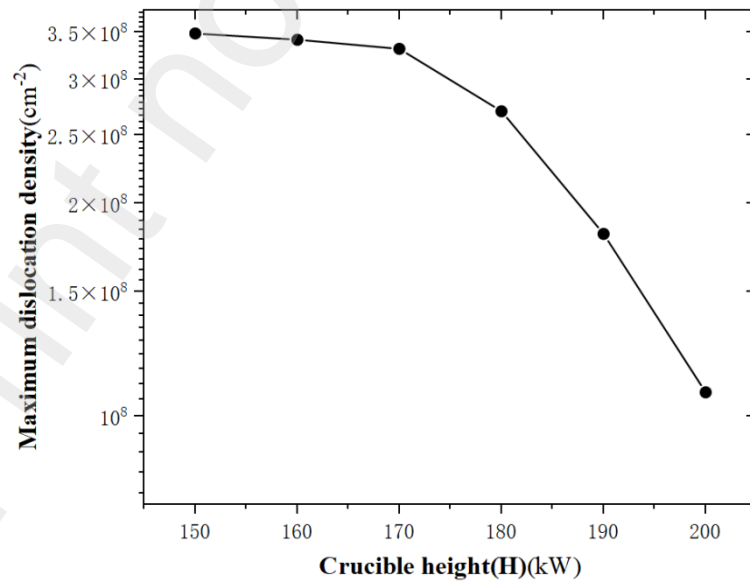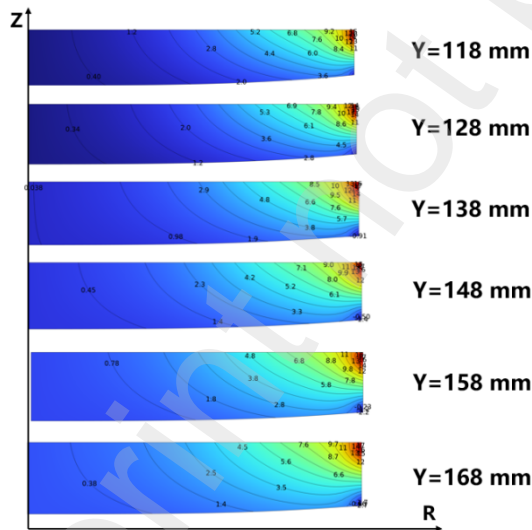


**Fig. 16** The correlation of heater power distribution and the maximum dislocation density of the grown crystal.

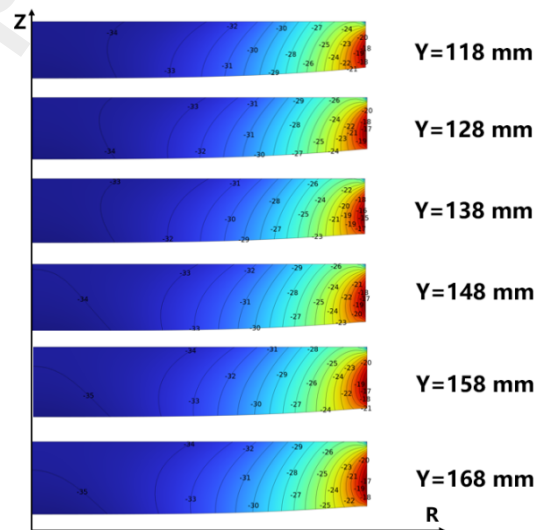# 3.3 The varying of distance between seed and powder

The last simulated parameter is the distance between the seed and SiC powder, which also indicates the amount of SiC powder to be injected. Setting three heater powers $P_1$=4 kW, $P_2$=4 kW, and $P_3$=19 kW, and adjusting the crucible height (H) to 160mm in order to modify the distance between the powder and seed. **Fig.17 (a)–(f)** shows the dislocation density(left) and absolute shear stress (right) of the crystal after growing 60h at various distance between seed and powder (Y). As shown in Fig. 15, the crystals grown exhibit a slightly convex shape, and the dislocation density maxima increases as the distance between the seed and the powder increases. By calculating radial average temperature difference ($\Delta T_x/L_x$) at various distance between seed and powder when growing 10h, where $\Delta T_x$ is the temperature difference between the edge and the center of the growing crystals, and $L_x$ is the length between the two. At 10 hours of growth, the approximate value of $L_x$ is equal to 100 mm. The $\Delta T_x/L_x$ value is 1.22, 1.15, 1.07, 1.02, 0.98, and 0.94 K/cm, with the distance between seed and powder being 118,128, 138,148,158, and 168 mm, respectively. $\Delta T_x/L_x$ reflects the uniformity of the surface temperature of the growing crystals, a small $\Delta T_x/L_x$ indicates lower isotherm line convexity, and a reduced temperature gradient in the radial direction along the growth interface. Therefore, according to the magnitude of the convexity of the crystal, the convexity of the six cases **(a)-(f)** gradually decrease. **Fig. 18** shows the radial temperature gradient distribution of the crystal after growing 60 h at various distances between seed and powder. It can be seen that the radial temperature gradient inside the crystal gradually increases with the distance (Y) between the seed crystal and the powder. **Fig.19** shows the distribution pattern of the axial temperature gradient in the crystal at different distances(Y), and there is no obvious difference in the axial temperature gradient, indicating that the formation of shear stress is mainly related to the radial temperature gradient. **Fig. 20** shows the correlation of the distance between seed and powder and the maximum dislocation density of the grown crystal. To better reveal the relationship between the temperature gradient, the stress, and dislocation density, the data is shown at a distance of 10 mm from the seed crystal surface for the three cases of Y=118, 138, 168 mm. The distributions in **Fig. 21(a)-(d)** shows the radial distribution of axial temperature gradient, radial temperature gradient, shear stress, and dislocation density. It can be seen from the plots that the radial temperature gradients are close for Y=168 and 138 mm. However, the axial temperature gradient is highest in the Y=168 mm case, resulting in the highest shear stress in the Y=168 case.

**Fig. 17** Dislocation density(left) and absolute of shear stress $\sigma_{rz}$(right) of crystal after growing 60h at various distance between seed and powder (Y):**(a)** 118mm; **(b)** 128mm; **(c)**138mm; **(d)** 148mm; **(e)** 158mm; **(f)**168mm.



**Fig.18** Radial temperature gradient distribution of crystal after growing 60 h at various distance between seed and powder (The unit of data is K/cm).

**Fig.19** Axial temperature gradient distribution of crystal after growing 60 h at various distance between seed and powder. (The unit of data is K/cm).
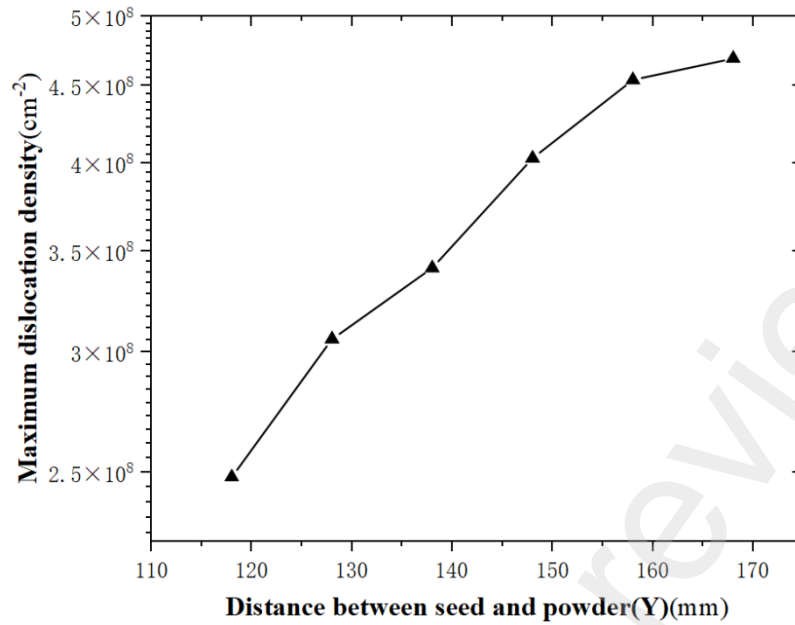
**Fig. 20** The correlation of the distance between seed and powder and the maximum dislocation density of the grown crystal.



**(a)**

**(b)**

**(c)**

**(d)**
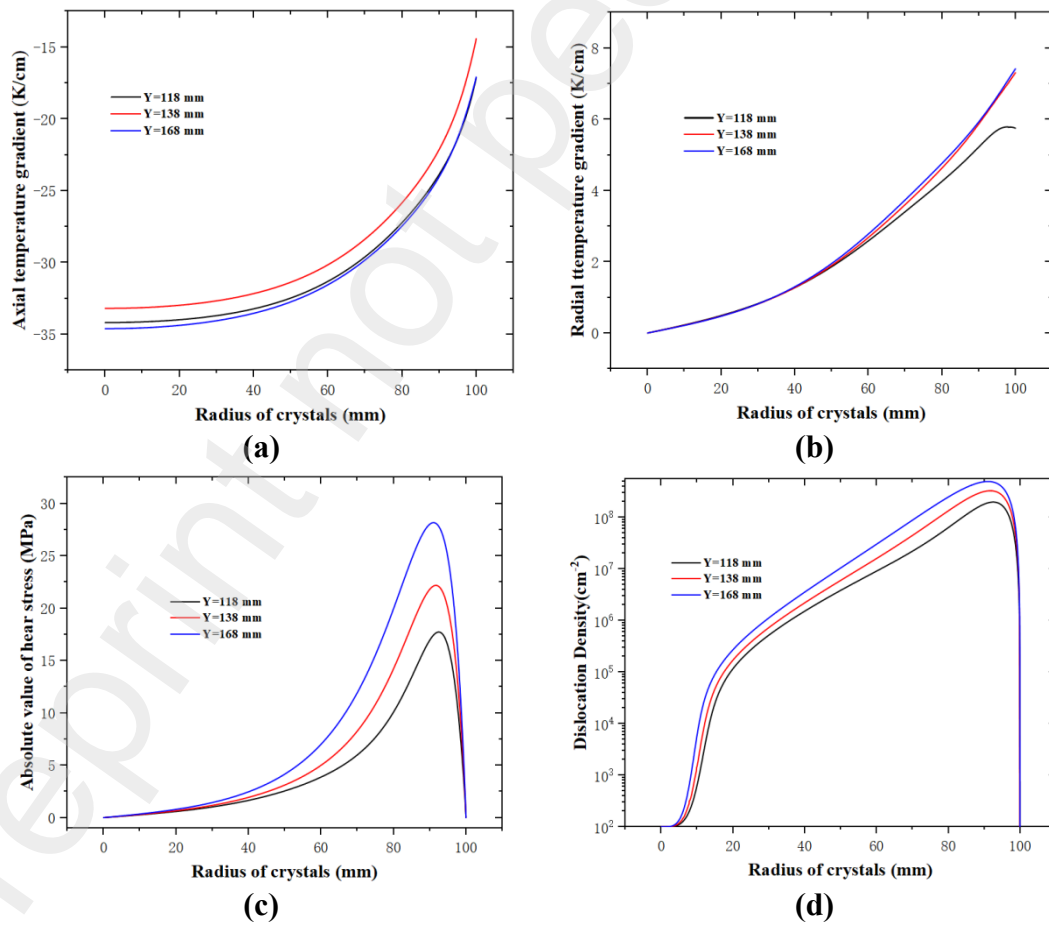
**Fig. 21** Temperature gradient, shear stress and dislocations at 10 mm from the seed crystal plane

for the three cases of Y=118, 138, 168 mm for the grown crystals: **(a)** axial temperature gradient;**(b)** radial temperature gradient; **(c)** absolute of shear stress $\sigma_{rz}$;**(d)** dislocation density

# 4. Conclusion

In this paper, finite element analysis of 200 mm SiC growth has been performed based on a "three-separation heater method" model for SiC crystal growth designed in previous work. Firstly, the transient thermal field of the growth process has been calculated, and the shape evolution of the crystal growth interface has been obtained using a growth rate equation combined with the dynamic mesh technique. The thickness and the shape of the grown crystals, as well as the distributions of the internal maximum shear stress and dislocation density, have been calculated for the variations of the distribution of the heating power, the height of the crucible, and the distances between the powder and the seed. The calculation results show that the heating power distribution has the most significant effect on the maximum values of stress and dislocation density. Different heating power distribution strategies enable the growth of SiC crystals with different convexities and the magnitude of thermal stresses are also different. Meanwhile, the shape and dislocation density of the crystals can be controlled by changing the crucible height. Finally, the dislocation density of the crystals grown with different distances between the seed crystals and powders has been calculated, and the analysis of the calculation results provides guidance for the growth of high-quality 200 mm SiC crystals to reduce the thermal stress and dislocation density.

# Acknowledgment

# Reference

[1] Y. Huang, R. Wang, Y. Qian, Y. Zhang, D. Yang, X. Pi, Theoretical study on the improvement of the doping efficiency of Al in 4H-SiC by co-doping group-IVB elements, Chinese Physics B, 31 (2022).

[2] A.A. Lebedev, V.E. Chelnokov, Wide-gap semiconductors for high-power electronics, Semiconductors, 33 (1999) 999-1001.

[3] K. Randall, Status of Silicon Carbide (SiC) as a WideBandgap Semiconductor for HighTemperature Applications: A Review, in: High-Temperature Electronics, IEEE, 1999, pp. 511-524.

[4] X. She, A.Q. Huang, O. Lucia, B. Ozpineci, Review of Silicon Carbide Power Devices and Their Applications, IEEE Transactions on Industrial Electronics, 64 (2017) 8193-8205.

[5] F. Wang, Z. Zhang, Overview of Silicon Carbide Technology: Device, Converter, System, and Application, CPSS Transactions on Power Electronics and Applications, 1 (2016) 13-32.

[6] P.G. Neudeck, J.A. Powell, Performance limiting micropipe defects in silicon carbide wafers, IEEE Electron Device Letters, 15 (1994) 63-65.

[7] B. Gao, K. Kakimoto, Three-Dimensional Modeling of Basal Plane Dislocations in 4H-SiC Single Crystals Grown by the Physical Vapor Transport Method, Crystal Growth & Design, 14 (2014) 1272-1278.

[8] C.X. YANG Xianglong, XIE Xuejian, PENG Yan, YU Guojian, HU Xiaobo, WANG Yaohao, XU Xiangang., Growth of 8 Inch Conductivity Type 4H-SiC Single Crystals, Journal of Synthetic Crystals, 51 (2022) 1745-1748.

[9] M. Musolino, X. Xu, H. Wang, V. Rengarajan, I. Zwieback, G. Ruland, D. Crippa, M. Mauceri, M. Calabretta, A. Messina, Paving the way toward the world's first 200mm SiC pilot line, Materials Science in Semiconductor Processing, 135 (2021).

[10] B. Xu, X. Han, S. Xu, D. Yang, X. Pi, Optimization of the thermal field of 8-inch SiC crystal growth by PVT method with "3 separation heater method", Journal of Crystal Growth, 614 (2023).

[11] A.S. Jordan, R. Caruso, A.R.V. Neida, A thermoelastic analysis of dislocation generation in pulled GaAs crystals, The Bell System Technical Journal, 59 (1980) 593-637.

[12] O.W. Dillon, Jr., C.T. Tsai, R.J. De Angelis, Dislocation dynamics during the growth of silicon ribbon, Journal of Applied Physics, 60 (1986) 1784-1792.

[13] N. Bános, J. Friedrich, G. Müller, Simulation of dislocation density: Global modeling of bulk crystal growth by a quasi-steady approach of the Alexander–Haasen concept, Journal of Crystal Growth, 310 (2008) 501-507.

[14] B. Gao, K. Kakimoto, Dislocation-density-based modeling of the plastic behavior of 4H–SiC single crystals using the Alexander–Haasen model, Journal of Crystal Growth, 386 (2014) 215-219.

[15] Q.-S. Chen, P. Zhu, M. He, Simulations of dislocation density in silicon carbide crystals grown by the PVT-method, Journal of Crystal Growth, 531 (2020)

125380.

[16] K. Kakimoto, S. Nakano, Numerical Analysis of Dislocation Density of SiC Crystals Tilted from [0001] Toward [1-210] and [1-100] Grown by Physical Vapor Transport, Crystal Research and Technology, 57 (2022).

[17] S.o. Lu, H. Chen, W. Hang, R. Wang, J. Yuan, X. Pi, D. Yang, X. Han, Numerical analysis of the dislocation density in n-type 4H-SiC, CrystEngComm, 25 (2023) 3718-3725.

[18] B.D. Nguyen, A.M. Rausch, J. Steiner, P. Wellmann, S. Sandfeld, , Journal of Crystal Growth, 532 (2020).

[19] H. Luo, X. Han, Y. Huang, D. Yang, X. Pi, Numerical Simulation of a Novel Method for PVT Growth of SiC by Adding a Graphite Block, 11 (2021) 1581.

[20] J. Drowart, G. De Maria, M.G. Inghram, Thermodynamic Study of SiC Utilizing a Mass Spectrometer, The Journal of Chemical Physics, 29 (2004) 1015-1021.

[21] S.K. Lilov, Study of the equilibrium processes in the gas phase during silicon carbide sublimation, Materials Science and Engineering: B, 21 (1993) 65-69.

[22] Z. Zhang, J. Lu, Q. Chen, V. Prasad, Thermoelastic stresses in SiC single crystals grown by the physical vapor transport method, Acta Mechanica Sinica, 22 (2006) 40-45.

[23] X.J. Chen, S. Nakano, L.J. Liu, K. Kakimoto, Study on thermal stress in a silicon ingot during a unidirectional solidification process, Journal of Crystal Growth, 310 (2008) 4330-4335.

[24] J. Fainberg, H.J. Leister, Finite volume multigrid solver for thermo-elastic stress analysis in anisotropic materials, Computer Methods in Applied Mechanics and Engineering, 137 (1996) 167-174.

[25] Z. Li, R.C. Bradt, The single crystal elastic constants of hexagonal SiC to 1000°C, International Journal of High Technology Ceramics, 4 (1988) 1-10.

[26] B. Gao, K. Kakimoto, Numerical Analysis of Impurities and Dislocations During Silicon Crystal Growth for Solar Cells, in: Y. Yoshida, G. Langouche (Eds.) Defects and Impurities in Silicon Materials: An Introduction to Atomic-Level Silicon Engineering, Springer Japan, Tokyo, 2015, pp. 241-272.

[27] N. Miyazaki, 26 - Thermal Stress and Dislocations in Bulk Crystal Growth, in: P. Rudolph (Ed.) Handbook of Crystal Growth (Second Edition), Elsevier, Boston, 2015, pp. 1049-1092.

[28] B. Gao, S. Nakano, H. Harada, Y. Miyamura, T. Sekiguchi, K. Kakimoto, Dislocation Analysis of a New Method for Growing Large-Size Crystals of Monocrystalline Silicon Using a Seed Casting Technique, Crystal Growth & Design, 12 (2012) 6144-6150.

[29] S. Karpov, A. Kulik, M. Ramm, Y. Makarov, Dynamics of 4H-SiC plasticity, Materials Science Forum - MATER SCI FORUM, 433-436 (2003) 297-300.

[30] Y.B. Yang, J. Wang, Y.M. Wang, Thermal stress simulation of optimized SiC single crystal growth crucible structure, Journal of Crystal Growth, 504 (2018) 31-36.